Super-Durable, Low-Wear, and High-Performance Fur-Brush Triboelectric Nanogenerator for Wind and Water Energy Harvesting for Smart Agriculture

Pengfei Chen, Jie An, Sheng Shu, Renwei Cheng, Jinhui Nie, Tao Jiang,*
and Zhong Lin Wang*

The triboelectric nanogenerator (TENG), as a promising energy harvesting technology, provides a new approach for the realization of the Internet of Things (IoTs). However, material abrasion severely limits its practical applications because of the deterioration in mechanical durability and electrical stability. Here, naturally available animal furs are introduced, owing to their superiorities of extremely low wear, high performance and humidity resistance. More than 10 times the electric output is observed relative to the conventional TENG, even at low driving torque. The transferred charge of fur-brush TENG (FB-TENG) exhibits only 5.6% attenuation after continuous operation for 300 000 cycles, maintaining high output performance even if the relative humidity increases up to 90%. Furthermore, a counter-rotating structure is first designed to further increase the output by doubling the relative rotation speed. Based on this mechanism, a significantly elevated output current of 36.6% is obtained in ambient conditions. Finally, self-powered automatic irrigation, weather monitoring and wireless water level warning multifunctional management systems are realized by collecting the wind and water flow energy. This work provides a strategy of reducing wear on the premise of high performance, which lays a foundation for effective environmental energy harvesting toward practical applications in big data and the IoTs.

1. Introduction

Agriculture, occupying the vast majority of gross national product, plays a vital role in the world economy development. For instance, the cultivated area of the United States is as high as 15.23 million square kilometers, and it is beyond half of the total land area in Bangladesh, Ukraine, and India, which are about 59.6%, 56.6%, 52.6%, respectively.[1] With the rapid development of information technology such as the internet of things (IoTs) and cloud computing, the modern agriculture is progressing to be smarter and more intelligent. Smart agriculture based on the IoT and big data technologies could provide precise planting management, all-round visual guidance, and intelligent production decisions through distributed data collection,[2] such as the temperature, humidity, and light intensity. In that way, the production efficiency and quality will be greatly improved. However, the feasibility and cost-effectiveness of agricultural IoTs have to be considered,[3] because of the batteries in the large number of widely distributed sensors needing to be replaced irregularly and the complex wiring in outdoor environments like large farmlands and terraces. It would be impossible to perform all these maintenance tasks by humans such as tracking, replacing, and handling the widely distributed batteries. A possible solution is to make each device self-powered by harvesting energy from the ambient environment.[4]

Recently, the self-powered system driven by triboelectric nanogenerator (TENG, also called as Wang generator) based on the coupling effects of contact electrification[5] and electrostatic induction[6] has drawn extensive attention.[7] TENG originating from the Maxwell's displacement current[8] can effectively harvest environmental mechanical energy to generate electricity from various sources,[9] such as wind,[10] human body motion,[11] and ocean waves,[12] etc. Meanwhile, it can also act as an active sensor without batteries for vibration sensing,[13] tactile mapping,[14] angle detecting,[15] and other movement related monitoring.[16] The self-powered systems composed of TENGs and sensors possess the ability of energy collection and environmental information monitoring. Compared with traditional

P. Chen, J. An, S. Shu, R. Cheng, J. Nie, Prof. T. Jiang, Prof. Z. L. Wang
CAS Center for Excellence in Nanoscience
Beijing Key Laboratory of Micro-nano Energy and Sensor
Beijing Institute of Nanoenergy and Nanosystems
Chinese Academy of Sciences
Beijing 100083, P. R. China
E-mail: jiangtao@binn.cas.cn; zhong.wang@mse.gatech.edu
P. Chen, J. An, S. Shu, R. Cheng, J. Nie, Prof. T. Jiang, Prof. Z. L. Wang
School of Nanoscience and Technology
University of Chinese Academy of Sciences
Beijing 100049, P. R. China
Prof. T. Jiang
Center on Nanoenergy Research
School of Physical Science and Technology
Guangxi University
Nanning, Guangxi 530004, P. R. China
Prof. Z. L. Wang
School of Material Science and Engineering
Georgia Institute of Technology
Atlanta, GA 30332-0245, USA

**ADVANCED
SCIENCE NEWS**
www.advancedsciencenews.com

**ADVANCED
ENERGY
MATERIALS**
www.advenergymat.de

electromagnetic generators (EMG), the TENG has merits of light weight, low fabrication cost, high efficiency, and versatile material and structure choices. Therefore, TENG exhibits irreplaceable advantages as the distributed energy source and active sensors in smart agriculture.

For practical applications of TENGs, the output performance and durability are two important concerns. As we know, the tribo-surface charge density dominating the TENG performance is dependent on the contact tightness between triboelectric materials. A closer contact can generate more triboelectric charges and higher output performance.[17] But the greater friction force between tribo-surfaces will bring the material abrasion and the decrease of device durability. Therefore, it is greatly desirable to develop the approaches to reducing the wear and improving the stability on the premise of output performance. Several attempts have been reported for enhancing the durability of TENGs. A rolling-electrification TENG by applying the rolling motion of steel rods on the dielectric surface was designed by Lin et al.,[18] indicating high energy conversion efficiency and high device durability due to the low frictional coefficient of rolling motion. Recently, pendulum inspired TENG structures have been prepared to reduce the material abrasion and enhance the device durability through the design of the air gap and flexible dielectric brushes.[19] However, their output performance is still limited by the small contact area and barren charge amount. In addition, Chen et al.[20] introduced a traction rope in rotational TENG to automatically adjust contact force between two friction layers according to the rotation speed, but the smaller transferred charge amount is still the biggest problem. Therefore, it is still a huge challenge to improve TENGs' output performance, durability, and wear resistance during long-time operation.

Herein, we developed a super-durable and low-wear TENG for efficient energy harvesting by utilizing animal furs as the triboelectric materials. Owing to the elasticity and softness, the animal furs can maintain tight contact and low friction state with other triboelectric materials during long-term operation to ensure high output performance and low wear. First, the output performance of the fur-brush TENG (FB-TENG) in a regular rotation motion at various magnitudes of torque was systematically measured, and the influences of environment humidity, material species, and structural parameter were also discussed. The performance of FB-TENG is hardly affected by the humidity change, even if the relative humidity is widely raised from 40% to 90%. A pair of meshing gear was also introduced to double the relative rotation speed between rotor and stator to further enhance the outputs. Then, the optimized FB-TENG was applied to harvest the wind energy and water flow energy at different wind speeds and flows. Finally, self-powered automatic irrigation, weather monitoring, and wireless warning systems were constructed by harvesting energy from wind and water flow, demonstrating the potential applications of the FB-TENG in agricultural big data and IoTs.

2. Results and Discussion

2.1. Structure and Working Principle of FB-TENG

In the smart agriculture, sensors and IoT devices are usually scattered all over the farmlands for wide monitoring of plant growth environment. Therefore, miniaturized and distributed energy supply is an important characteristic of the future agricultural IoT systems. **Figure 1**a depicts prospective applications of the FB-TENG by scavenging environmental mechanical energy to provide distributed power supply for electrical devices in agricultural production. The water flow energy in the irrigation canals or rivers and wind energy can be continuously harvested by the waterwheel FB-TENG and widely-distributed wind energy collection columns to power many kinds of sensors to realize real-time environmental monitoring and fully-automated agricultural management. The schematic structures of the waterwheel and wind energy collection column are visualized in Figure 1b,c. Each FB-TENG unit adopting a freestanding mode, which is packaged in a water-proof acrylic shell, is composed of a fur disk and an electrode disk attached by the polytetrafluoroethylene (PTFE) film, as sketched in Figure 1e. Such waterwheel FB-TENG for water flow energy harvesting consists of two parallel sections: the left main body of generator with five arrayed FB-TENG units connected in parallel and the right ordinary waterwheel with reversing gears. Here, a pair of meshing gears is applied to make two kinds of triboelectric disks rotate in different directions. All the fur disks are fixed on the acrylic shell and directly driven by the water flow to rotate in an anticlockwise direction, while the electrode disks are locked on the central shaft and driven by the reversing gears to rotate in a clockwise direction. The relative rotation between the fur disks and electrode disks by adding an ordinary waterwheel can multiply the output performance of TENGs (Note S1, Supporting Information). Similarly, in the wind energy collection column, the relative movement can be achieved by a planetary gear mechanism as shown in Figure 1d and Note S1 (Supporting Information).

Figure 1e presents the structural details of a TENG unit, in which four sectored furs are arrayed in a circle on the acrylic substrate, which is fixed to the generator shell by bolts. Soft animal fur is not only a kind of excellent electropositive material, similar to the human hair,[21] but also has low friction resistance (Figure S2, Supporting Information). The electrode disk with four pairs of complementary electrodes was fabricated using the printed circuit board (PCB) technology. Two groups of copper sectors are respectively connected electrically. The detailed fabrication process can be found in the Experimental section. The basic working mechanism of the FB-TENG was illustrated in Figure 1f. The triboelectrification between the fur brushes and the PTFE film generates positive electrostatic charges on the furs and negative charges on the PTFE surface. Owing to the charge conservation, the total tribo-charge amounts on the fur sector and PTFE are equivalent. The stages 1–4 in Figure 1f represent a typical working cycle of the freestanding FB-TENG. With the relative rotation of the fur disk and electrode disk, free charges on the electrodes will be redistributed between two groups of electrodes through the external load to balance the change of potential difference, according to the electrostatic induction. The induced periodically transferred charges between two groups of electrodes will produce AC output due to the periodic structure.

2.2. Electrical Characterizations for the FB-TENG

In order to investigate the influence of fur species on the output performance of FB-TENG, several common animal furs
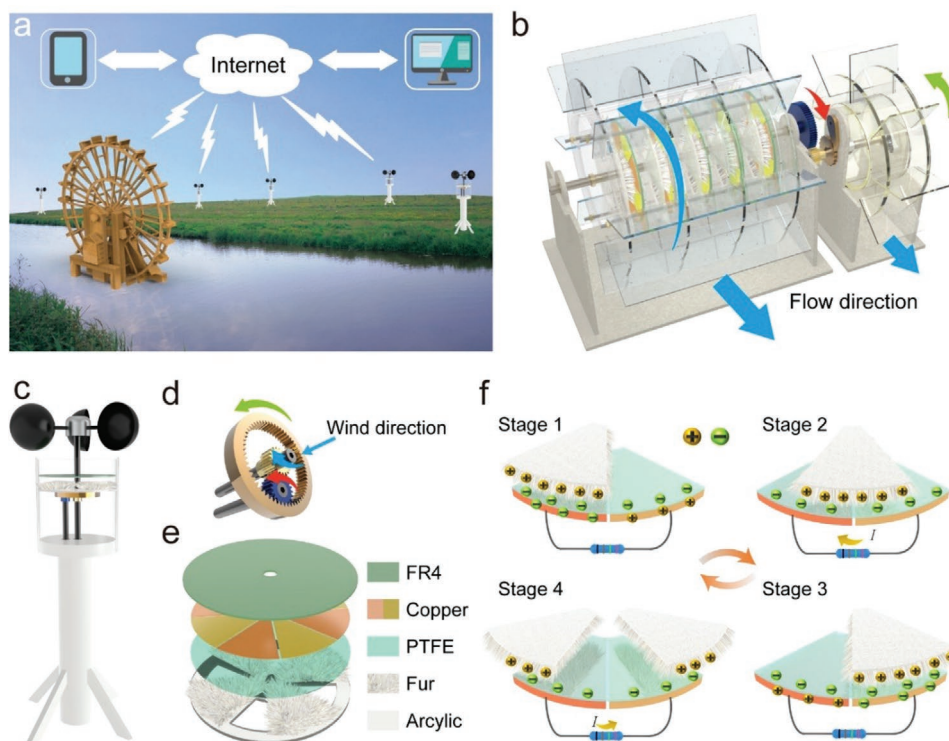
Figure 1. Application, architecture and mechanism of the FB-TENG. a) The concept proposed for applying the FB-TENG in field of smart agriculture. b) Illustrations of waterwheel structure for water flow energy harvesting, which consists of two sections: the left-hand section is the generator, including five arrayed units of FB-TENG, and the right-hand one is the reversed side, which is used to provide reverse force for "stator" of TENG. c) Schematic diagram of the energy harvesting column for wind energy. d) An enlarged schematic diagram of the reversed structure used in (c). e) Material composition of the FB-TENG, including electrode disk and fur disk. f) Schematics of the four stages in one full electricity-generating cycle focusing on the charge distributions at the two sector-electrodes.

obtained from rabbits, sheep, and dogs were selected for comparison. A standardized dynamic torque measurement system, as schematically shown in **Figure 2**a, was established to explore the relationship between the friction torque and the TENG outputs for different triboelectric materials. The electrode disk is fixed on the optical platform, while the rotating fur disk is fixed on the step motor through a torque meter, which is used to measure the friction force in real time. The step motor and dynamic torque sensor are mounted on an *XY*-direction platform to fine-tune the relative position of two disks for convenient adjustment of friction torque. During the measurements, real-time friction torque can be displayed and recorded by the computer as illustrated in Figure S3 (Supporting Information). The rotating speed was chosen as 120 rpm, which is close to the water flow speed in natural rivers, in the following experiments besides when studying the effect of the rotating speed. Figure 2b shows the photographs of the fur disks with different animal fur materials, as well as a common copper disk as rotor for comparison, in which a sponge is embedded between the copper film and acrylic substrate to ensure a similar flexibility with the fur disk. The transferred charge, output current, and output voltage of the FB-TENG with several common animal furs as functions of the torque are presented in Figure 2c,d and Figure S4a (Supporting Information). As can be seen, the charge, current, and voltage all increase with increasing the torque, because of more sufficient surface contact at a

larger torque. The rabbit FB-TENG exhibits the highest outputs of 1260 nC, 28 µA, and 3750 V at 1.0 N m among the four TENGs (Figure 2e,f; Figure S4b, Supporting Information), which is associated with the highest fur density for the rabbit fur (Figure S5, Supporting Information).[22] It is worth noting that, at lower torque conditions (0.05, 0.1, 0.2 N m), the transferred charge of TENG can be increased by more than ten times through replacing copper layer by animal fur, as shown in Figure 2g. In addition, the surface charge densities of the TENGs with rabbit fur and copper at different torques were compared with previous grating structure TENGs using copper,[23] as shown in Figure 2h. The FB-TENG with rabbit fur generates much higher charge density, and the maximum value can reach 115.2 µC m^{-2}. Therefore, achieving high output performance at low torque is one of the unique advantages of the FB-TENG, which will find wider applications, especially in the case of low driving force.

Besides the torque, the relative humidity (RH) of the environment is another important factor that affects the output performance of TENGs. In previous works, the humidity was found to sharply decrease the surface charge density above 50% RH.[24] Here, the relationship between the output performance of rabbit FB-TENG and relative humidity are systematically studied, as shown in **Figure 3**a–c. Since the performance improvement is not obvious when the torque is greater than 0.6 N m, the selection of the torque of 0.6 N m is sufficient to show the influence of
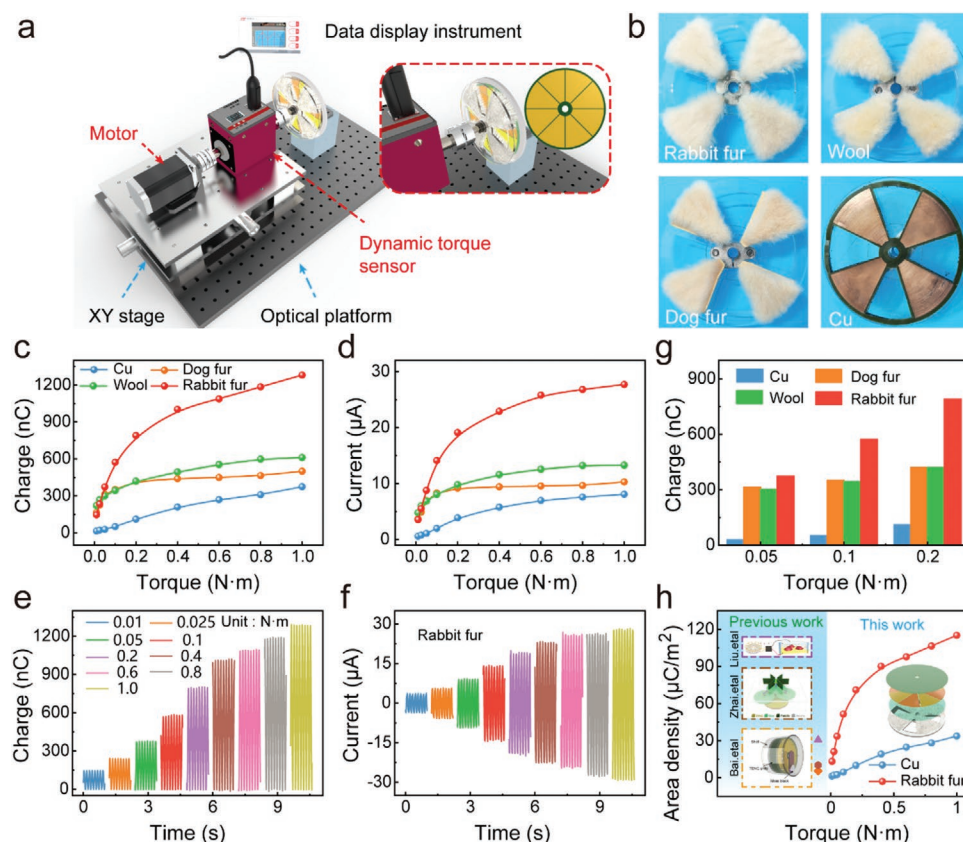
ADVANCED
SCIENCE NEWS
www.advancedsciencenews.com

ADVANCED
ENERGY
MATERIALS
www.advenergymat.de

Figure 2. Influences of torque and materials on the output performance of TENG at 120 rpm. a) Schematic diagram of the dynamic torque measurement system. The inset is an enlarged view of the measurement part in the system and the electrode disks. b) Photographs of the rotors with different types of animal's fur brushes or copper employed in the FB-TENG. c) Transferred charge and d) output current of the FB-TENG with various materials as functions of the torque ranging from 0.01 to 1.0 N m. e) Transferred charge and f) output current of the FB-TENG with rabbit fur with respect to the torque. g) Comparison of the transferred charge of the FB-TENG with various materials at lower torque (0.05, 0.1, 0.2 N m). h) Comparison of the generated surface charge density of the present TENG using the rabbit fur and copper under different torques with previous grating structure TENGs using copper. The negative triboelectric materials used in the tests are all PTFE. The ambient humidity during the measurement is 40%.

other parameters. When the average humidity measured varies from 40% to 90% and remains (Figure S6, Supporting Information), there is almost no attenuation in the transferred charge and output current under the conditions of 0.6 N m and 120 rpm. With a continuous increase in RH, the transferred charge also has only a slight decrease. At high RH condition, the output performance of FB-TENG can maintain stable for more than 10 min. The FB-TENG is insensitive to the humidity, maybe because of the poor wettability of rabbit fur due to its denseness and surface scale layer.[25] Such property breaks the limitation of negative effects of humidity on the TENG performance, which will further expand the practical applications of FB-TENG especially in the environment with sudden changes in humidity. On the other hand, previous studies have shown that the temperature has almost no effect on the output of the nanogenerator when the temperature is below 353 K.[26] For other harsh environments such as low temperatures and acid rains in actual weather, we can overcome the possible influences or damages by choosing high-quality insulation materials and corrosion-resistant materials. This shows that our equipment is highly reliable because it can operate stably in harsh environments.

Subsequently, the effects of the rabbit fur length, rotating speed, and grating number on the performance of the FB-TENG were investigated, as demonstrated in Figure 3d–f. It is apparent that the fur length has little effect on the transferred charge due to the same fur density. And also, the charge is basically unchanged, as the rotating speed increases from 30 to 300 rpm (Figure S7, Supporting Information). But the output current increases almost linearly, reaching 65 μA at 300 rpm, because the output current is related to the relative motion velocity according to $I = \mathrm{d}Q/\mathrm{d}t$.[27] Similarly, the current can be increased by raising the grating number, which arrives at 55 μA for a grating number of 16 at 120 rpm. Faster relative motion means faster charge transfer and higher average output power. So, increasing the relative motion is an effective way to improve the TENG performance, which is why we introduce a pair of gears to drive the electrode and fur disks rotate at different directions.

Furthermore, the durability tests were performed to reveal the output stability of the rabbit FB-TENG, as shown in Figure 3g. There is only a minor attenuation of about 5.18% under uninterrupted operation for more than 13 000 cycles at 0.6 N m, and the transferred charge also has a slight decrease of 5.6% after
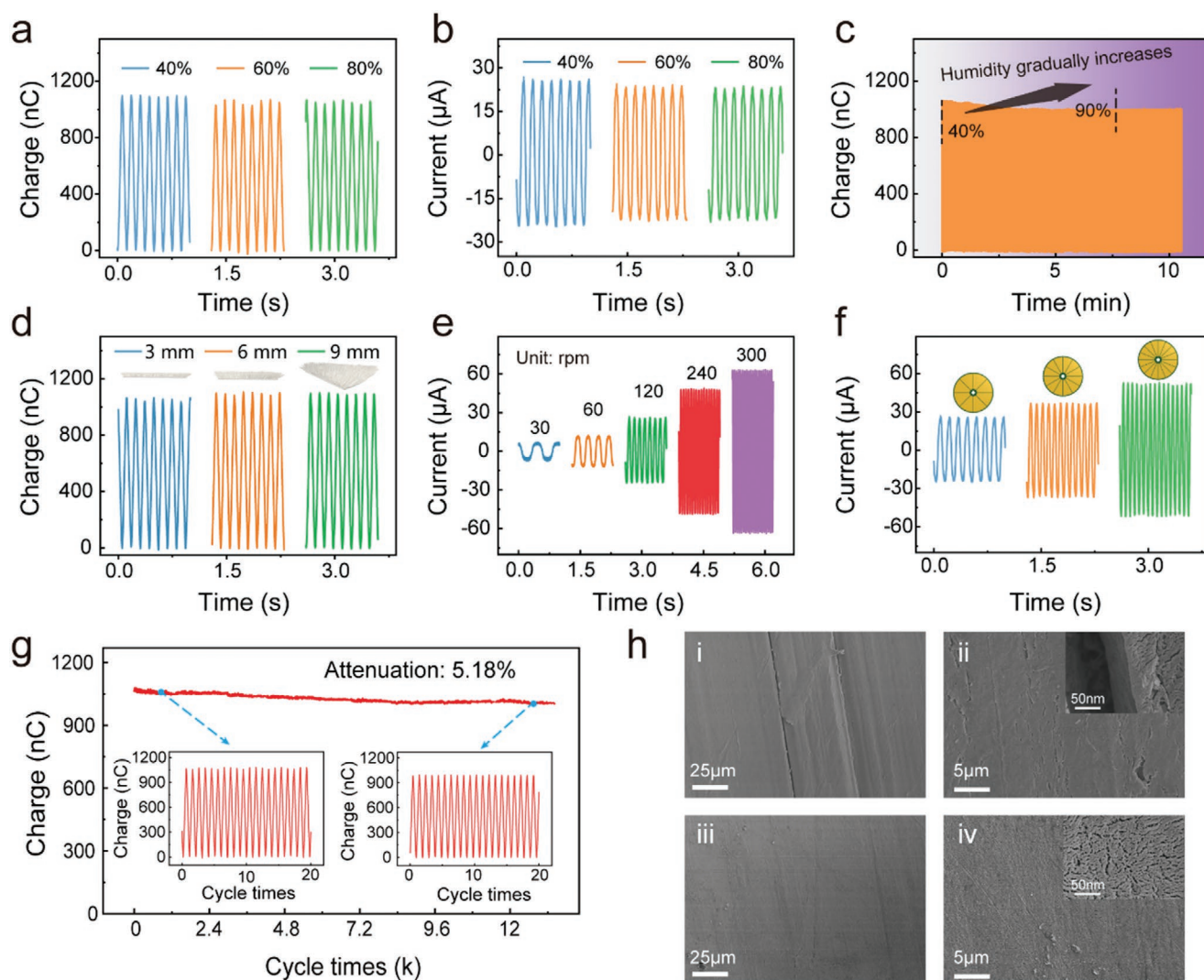
**ADVANCED
SCIENCE NEWS**

www.advancedsciencenews.com

**ADVANCED
ENERGY
MATERIALS**

www.advenergymat.de

Figure 3. Basic output characteristics and durability of the FB-TENG with rabbit fur at 0.6 N m. a,b) Effects of the environment humidity on a) transferred charge and b) output current of the FB-TENG. c) The change of transferred charge with the continuous increase in humidity for more than 10 min. d) Transferred charge of the TENG for different fur lengths at 120 rpm. e,f) Output current of the TENG at various rotating speeds and grating numbers for the fur length of 9 mm. g) Variation of the transferred charge amount under continuous measurement for 13 000 cycles. h) Comparison of SEM images for the PTFE film surfaces rubbed by Cu (i–ii) and rabbit fur (iii–iv) after 72 000 cycles of continuous testing.

continuous operation for 300 000 cycles at 0.1 N m (Figure S8, Supporting Information), implying the excellent charge retention ability of the FB-TENG. Then the mechanical durability was also evaluated by comparing the surface abrasion degree of PTFE material after 72 000 working cycles, as indicated in Figure 3h. Compared with unused commercial PTFE film (Figure S9, Supporting Information), the PTFE surface rubbed by the Cu is severely worn out, and many scratches appear on the surface. Thus, its output performance has dropped sharply. There is a performance degradation of 20.1% after 13 000 cycles (Figure S10, Supporting Information). This is because the worn PTFE membrane debris is adhered to the Cu, which reduces the surface potential of the Cu, thereby affecting its performance. On the contrary, nearly no damage can be found on the PTFE surface rubbed by rabbit furs for 72 000 cycles, and the surface topography becomes more delicate and flat than original PTFE

film, owing to the high density and softness of fur-brush. These advantages of lower resistance force, less wear, higher output, and stronger humidity resistance make the FB-TENG act as a superior candidate for environment energy harvesting.

2.3. Application of FB-TENG for Wind Energy Harvesting

To demonstrate the applications of the FB-TENG in environmental energy harvesting, an energy harvesting column for wind energy was fabricated and investigated. **Figure 4**a shows the photograph of as-fabricated wind energy harvesting device. Here, a planetary gear mechanism is adopted to provide the reversed force for the fur disk to increase the relative movement between two disks. The electrical outputs of the rabbit FB-TENGs with or without a reversed structure

ADVANCED
SCIENCE NEWS
www.advancedsciencenews.com

ADVANCED
ENERGY
MATERIALS
www.advenergymat.de

were compared at different wind velocities, as presented in Figure 4b,c. As the wind velocity increases from 8 to 23 m s^{-1}, the peak values of transferred charge are basically constant at 0.4 µC for the two kinds of structures, while the peak current increases for both of them. At the wind velocity of 23 m s^{-1}, the output current with reversed structure can reach 65.4 µA and has an increase of 32.2% compared to the TENG without reversed structure, which is consistent with the derivation in Note S1 (Supporting Information). That means under the same external triggering, the reversed structure will greatly increase the output power of FB-TENG. At a low wind velocity, the output current without the reversed structure is higher, because the damping is introduced by the planetary gear structure. However, these can be solved by improving the manufacturing process.

In order to better demonstrate its application in the laboratory environment, we chose a wind speed with a larger output current to shorten the charging time of the capacitor. On the other hand, this also proves that the wind energy collection column we designed can work stably in harsh natural environments and has good working reliability. Figure 4d shows the peak current, peak and average power behaviors with respect to the load resistance for the wind energy collected column equipped with reversed structure at the wind velocity of 23 m s^{-1}. The average power can be obtained by calculating the energy through the resistance in a unit time according to the following Equation

$$P_{ave} = \frac{\int_0^T I(t)^2 \, R \mathrm{d}t}{T} \tag{1}$$

where the $I(t)$ is the current across the resistor at the time t, R is the resistance, and T is the integration time. It can be found the maximum peak power of 56.79 mW and maximum average power of 28.03 mW can be achieved at the matched resistance of 30 MΩ. Accordingly, the peak power density and average power density can be calculated to be 5.02 and 2.40 W m^{-2}, respectively. The charging performance of the device was also explored, as presented in Figure 4e. The voltage on the capacitor of 220 µF can be charged to 9 V within 45 s, showing excellent energy harvesting ability.

Subsequently, we demonstrated the applications of the wind-driven FB-TENG as a distributed energy source to realize smart agriculture and precise agriculture. Figure 4f is a schematic circuit diagram of simulated automated irrigation system powered by the FB-TENG. In this system, the soil moisture sensor can transmit the soil moisture signals to the water pump control unit (PCU) to realize the fully-automated irrigation. A 470 µF capacitor is used as an energy storage and buffer unit to power the soil moisture sensor, because it cannot be directly powered by the TENG. When the soil moisture is lower than the normal, the capacitor can be rapidly charged to 5 V within 45 s, then the switch is closed, and the sensor is powered to transmit moisture signals to the controller. Once the controller receives the low moisture signal, it will control the irrigation pump to work until the soil moisture arrives at a normal value. The voltage profile of this process is illustrated in Figure 4g. If the soil moisture is in the normal range, the sensor powered by the FB-TENG can work continuously to monitor the soil moisture in

real time (Figure 4h). The experiment processes are recorded in Movies S1 and S2 (Supporting Information), and the insets of Figure 4g,h. Similarly, the FB-TENG can also harvest the wind energy to power the raindrop sensor for continuously monitoring the weather and giving an alarm when it rains as illustrated in Figure 4i and Movie S3 (Supporting Information). Here, a Zener diode of 6.1 V is applied to prevent the capacitor from being overcharged, because there is no energy consumption when there is no rain. The insets illustrate the states of continuous monitoring when there is no rain and alarming when the weather is rainy. The detailed circuit diagram for powering the raindrop sensor is plotted in Figure S11a (Supporting Information).

Besides monitoring the soil moisture and weather, other environmental parameters can also be characterized by this platform such as the temperature and RH value. From the measured charging curve in Figure 4j, it can be found that two serial-connected thermo-hygrometers are able to work constantly under the power supply of FB-TENG. Interestingly, the voltage on the capacitor when powering the thermo-hygrometers is still rising, implying that the energy harvesting speed exceeds the consumption speed. The whole working process of the thermo-hygrometers is recorded in Movie S4 (Supporting Information). In addition, 900 light-emitting diodes (LEDs) are also directly lighted up by the FB-TENG. The snapshot and movie are shown in Figure 4k and Movie S5 (Supporting Information).

2.4. Application of FB-TENG for Water Flow Energy Harvesting

Monitoring of irrigation canals or rivers is an indispensable part of agricultural production. Some necessary information, such as water temperature, water level, electrolyte, and other parameters, can be obtained through building a basic network and installing sensors in the detection area, which can provide timely early warning for the growth of crops and provide support for the timely protection of crops and improve production efficiency. In this demonstration, a waterwheel structure FB-TENG with rabbit fur was fabricated to realize all-round and all-information intelligent management by collecting the water flow energy. The device includes the left-hand generator with five arrayed FB-TENG units connected in parallel, and the right-hand ordinary waterwheel in which the fur disk rotates in the opposite direction with respect to the electrode disk. **Figure 5**a shows the photograph of the waterwheel device placed on the water flow channel of simulated river. The meshing gears are highlighted and enlarged. The transferred charge and output current of the waterwheel FB-TENG with and without reversed structure for different water flow are shown in Figure 5b–d. The transferred charge remains stable around 3.0 µC for both structures, because it is only dependent on the torque for the same triboelectric material. An approximately linear relationship between the output current and water flow can be observed (Figure 5b), since the increase in the water flow can accelerate the rotation of the waterwheel. And the reversed structure can increase the output current from 34.2 to 46.6 µA (about 36.3% enhancement) at 85 m^3 h^{-1}. The 3.3 mF capacitor can be rapidly charged to 6.2 V within 80 s with the charging rate
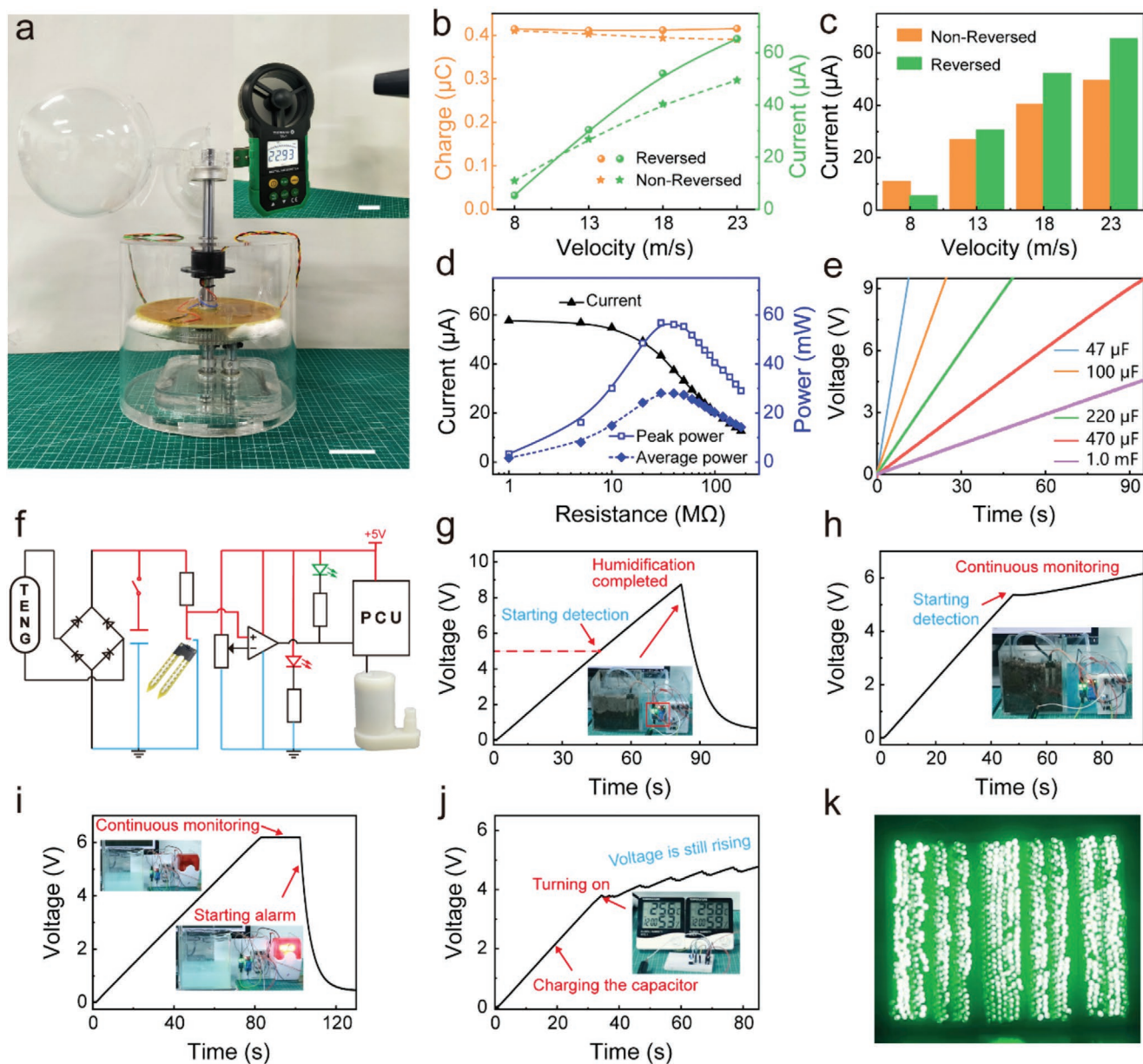
Figure 4. Application demonstrations of the FB-TENG for wind energy harvesting. a) Photograph of the as-fabricated wind energy collecting column. The inset shows the measured wind speed. The scale bar is 3 cm. b) Transferred charge and output current of the wind energy harvesting device with or without reversed structure under different wind speeds. c) Comparison of the current for the TENG with or without reversed structure through the column graphs. d) Peak current, peak power, and average power of the TENG with respect to the load resistance under the wind blowing of 22.93 m s^{-1}. e) Charging voltage on various capacitances for the wind-driven FB-TENG. f) Schematic circuit diagram of self-powered soil moisture monitoring system. g) Voltage profile on a 470 μF capacitor charged by the TENG to power the soil moisture sensor, which can start the water pump to complete humidification when the soil moisture is lower than normal. The inset is the photograph showing that the soil is successfully humidified. h) Voltage on the capacitor at the continuous monitoring of soil moisture when the soil moisture is normal. The inset is the photograph of soil with normal humidity. i) Voltage profile for continuously monitoring the weather and giving an alarm when it rains. The insets illustrate the states of continuous monitoring when there is no rain and alarming when the weather is rainy. j) Charging curve of a 470 μF commercial capacitor when powering two serial-connected hygro-thermographs, driven by the FB-TENG in wind. The inset is the photograph showing the room temperature and humidity. k) Photograph of 900 LEDs lighted directly by the FB-TENG.

of 0.255 mC s^{-1} by the reversed structure device (Figure 5e). We believe that the performance of FB-TENG will become more outstanding by introducing the power management. Then the resistance dependence of the outputs for the water-wheel FB-TENG was also characterized at 100 m^3 h^{-1}, as shown

in Figure 5f. The peak power arrives at the maximum value of 30.35 mW at 18 MΩ, while a maximum average power of 18.70 mW can be obtained, which is about 62% of the peak power. Here, the average power shows less decaying relative to the peak power, since the current waveform of FB-TENG is
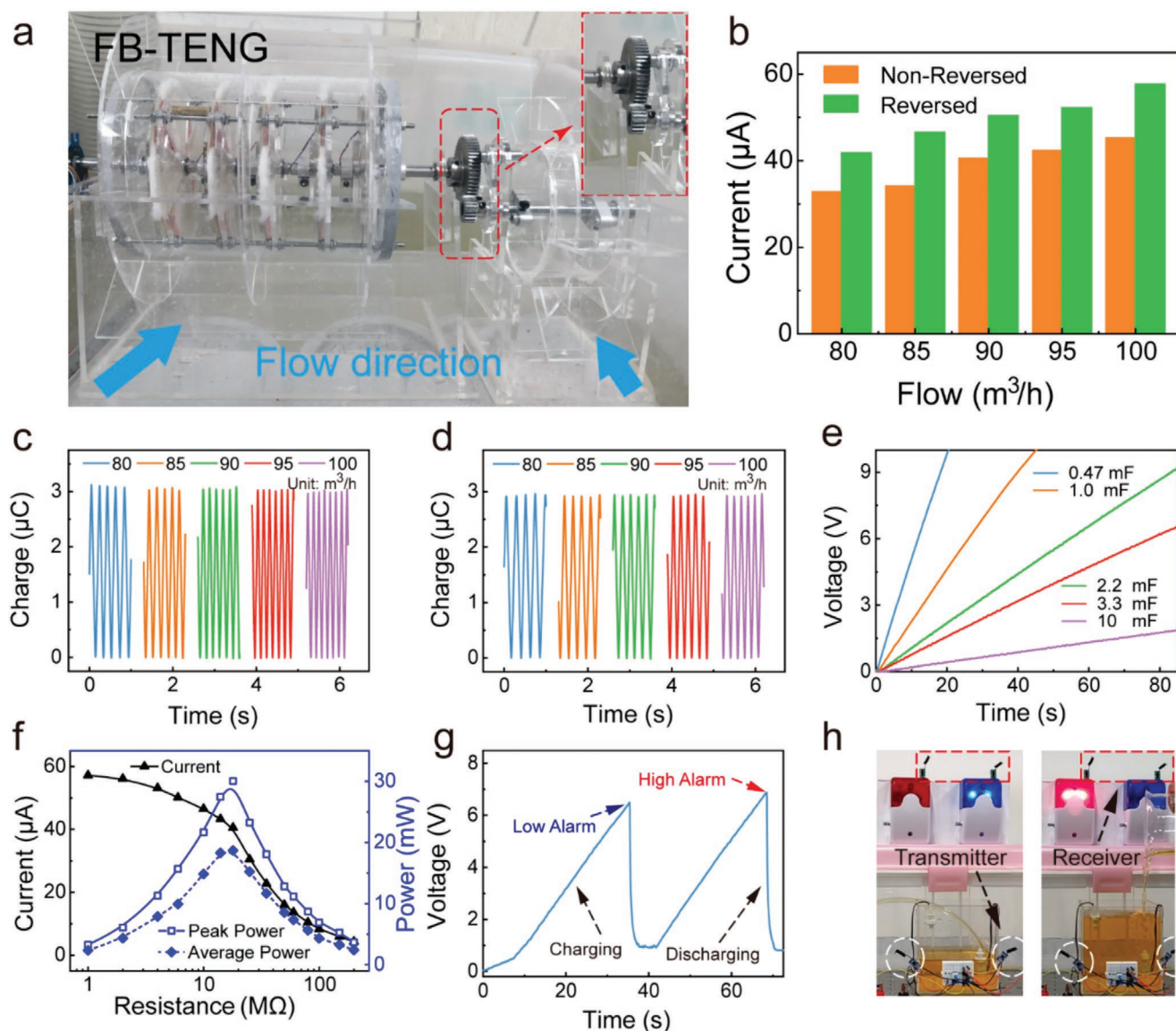
Figure 5. Application demonstrations of the FB-TENG for water flow energy harvesting. a) Photograph of the fabricated waterwheel with reversed structure placed on the water flow channel. The image highlighted by red dashed lines is meshing gear. b) Comparison of the current with or without reversed structure under different flows. c,d) Transferred charge of the waterwheel TENG with and without reversed structure under different flows. e) Charging voltage on various capacitances for the FB-TENG at the flow of 100 m^3 h^{-1}. f) Peak current, peak power, and average power of the TENG with respect to the load resistance at 100 m^3 h^{-1}. g) Charging and discharging process for a capacitor of 1 mF to power the transmitter for completing the high and low alarm of the water level. h) Photograph of low and high-water level alarm.

close to sine wave rather than pulse wave. According to the device area, the peak power density and average power density are obtained to be 0.54 and 0.33 W m^{-2}, respectively.

Based on the excellent performance of the waterwheel FB-TENG, a self-powered wireless water level monitoring and warning system through water flow energy harvesting is constructed for monitoring the water level in real time, which can serve as an early warning of drought and flood. The water level control system introduces two level float switches at low and high levels in the water tank for autonomous control, marked as S1 and S2, respectively. The S1 and S2 are connected with the low transmitter (LT) and high transmitter (HT), respectively, which are powered by the FB-TENG through a 1 mF

capacitor. The specific circuit diagram is drawn in Figure S11b (Supporting Information). At a normal water level, both switches are normally in the open state, and the 1 mF capacitor is charged by the FB-TENG to store the electric energy for use at critical moments. When the water level drops to the lowest level due to drought or other reasons, the normally-open switch S1 closes, and the LT is powered up by the capacitor discharging to send a signal to the receiver for low water level alarm with sound and light, as can be seen from the left side of Figure 5h. After that, we supplemented water into the water tank to reveal the principle of high water level alarm. Similarly, the capacitor is first charged until the highest water level, at which the capacitor is discharged to power the HT due to the close state of the

ADVANCED
SCIENCE NEWS

www.advancedsciencenews.com

ADVANCED
ENERGY
MATERIALS

www.advenergymat.de

switch S2. The charging and discharging process of the 1 mF capacitor are shown in Figure 5g and Movie S6 (Supporting Information).

3. Conclusions

In summary, we constructed a FB-TENG based on the naturally available animal furs to effectively harvest the wind and water flow energy. Compared with traditional copper, the outputs of TENG with the fur brushes can be increased by more than ten times under the same torque. The FB-TENG exhibits strong robustness and durability due to the little friction and wear from the soft furs, and there is only 5.6% attenuation in the transferred charge at 0.1 N m after operating continuously for 300 000 cycles. Importantly, the FB-TENG is not sensitive to the change of environmental humidity due to the denseness of furs. The output performance can remain stable even if the relative humidity is widely changed from 40% to 90%. Furthermore, the output current of FB-TENG can be increased by 36.6% through the relative rotation of fur disk and electrode disk realized by the counter-rotating structure, accompanied by a great enhancement in output power. Based on the optimized FB-TENG with column and waterwheel structures, we built the self-powered automatic irrigation, weather monitoring, and wireless warning systems by wind and water flow energy harvesting. This work could provide an approach to improving the durability and output performance of TENGs, expanding their applications in field of smart agriculture.

4. Experimental Section

Fabrication of FB-TENG Unit: The TENG unit is composed of two parts: a fur disk and an electrode disk. For the fur disk, four sectored furs with equal-degree radially-arrayed sectors were pasted on the acrylic substrate. The outer diameter and inner diameter of the sectored furs are 120 and 23 mm, respectively. All furs in the experiments were got from the back of the animal to ensure a uniform density. The furs with the lengths of 3, 6, and 9 mm were obtained by trimming. It is worth noting that as a mature product, animal fur is very easy to obtain from the market at low price, for example, the price of rabbit fur is 30 dollars per square meter. Here, the fur was chosen that integrates hair and skin, which was obtained after a series of treatment processes, such as tanning. After processing, the skin of rabbit fur was about 1 mm-thick, while the skins of wool and dog fur are thicker (about 1.5–2 mm). An acrylic sheet was cut into the desired shape by a laser cutter (PLS6.75), and the acrylic surface uncovered by furs was hollowed out as shown in Figure 2b. Similarly, the furs were also cut into the target shape by laser cutter, and then double-sided tape (3M LSE) was used to attach it on the acrylic substrate. For the electrode disk, the epoxy glass fiber substrate (120 mm in diameter) with copper layers (35 μm in thickness) was fabricated by the PCB technique. The patterned Cu sectors were divided into two groups, which were electrically connected respectively. Then the 80 μm-thick PTFE films were adhered on the copper layers as the triboelectric layer.

Fabrication of Waterwheel Structure: The waterwheel structure consists of two sections: the generator section on the left-hand, including five arrayed units of FB-TENG and the ordinary waterwheel section on the right-hand, which was used to provide reverse force for the "stator" of TENG unit. For the generator section, the acrylic cylindrical shell with a length of 20 cm, a thickness of 3 mm, and an outer diameter of 15 cm was prepared as a waterproof chamber to accommodate TENG units.

Two end-caps embedded with two bearings were integrated with the cylindrical shell on its top and bottom sides, followed by the sealing and waterproofing process using polymer glues. A stainless-steel shaft ran through the whole structure as a rotation shaft and the driven gear with 80 teeth was fixed at one end. Each fur disk base had a diameter of 135 mm with a central hole of 10 mm to hold the bearing. And a through hole of 4 mm was drilled on the edge of each fur disk base for connection by bolts and spacers and fixing it with the two end-caps to achieve simultaneous rotation with the cylindrical shell. All the electrode disks were fixed onto the central shaft by the shaft lock and driven by the gear. Five basic TENG units were electrically connected in parallel and collected the electrical energy through conductive slip rings. For the ordinary waterwheel section, a cylindrical shell with a length of 5 cm, a thickness of 5 mm, and an outer diameter of 11 cm were integrated with two end-covers. And all of them were fixed on the ordinary waterwheel shaft by the shaft lock. A gear with 20 teeth was fixed on one end of the shaft as a driving gear to transmit reversing force. For the driving blades, the generator section contains four hollow disks and eight rectangle blades to convert water flow into a rotation motion. Similarly, there are two hollow disks and eight rectangle blades on the ordinary waterwheel section.

Fabrication of Wind Energy Collection Column: The electrode disk, the sun gear with 20 teeth, and the wind cup were all fixed on the same central shaft, and driven by the wind. The fur disk base had a diameter of 130 mm with a center hole of 10 mm to hold the bearing, and was glued with the ring gear with 60 teeth to maintain the same rotation. A round acrylic base embedded in two bearing seats was used to support the planetary shaft and central shaft. And the conductive slip ring was used to collect electrical energy. All of the above, except for the wind cup, were placed in a cylindrical shell with the length of 15 cm. The related electrical components used to develop a schematic circuit diagram of a simulated automated irrigation system include energy storage capacitor, commercial resistive soil moisture sensor, voltage comparator (LM393), sensor divider resistor (10 kΩ), and potentiometer (10 kΩ) for adjusting the sensitivity of the sensor. Soil moisture will cause different resistances of the sensor. After processing by the voltage comparator, the switch of the water pump will be automatically controlled by the PCU (relay).

Electric Measurements of the TENG Device: The water flows applied in this work were generated by a water pump (maximum flow: 160 m³ h⁻¹) and controlled by a frequency converter (VFD075M43A). The wind was produced by a commercial air blower, and the wind speed was tested by an anemometer (THINRAD TA-1). The humidity was controlled by a humidifier, and stabilized for more than 12 h. The torque was measured by a commercial torque sensor (DYN-200). The transferred charge and output current were measured by a current preamplifier (Keithley 6514 System Electrometer), while the output voltage directly produced by the FB-TENG was measured using a high-voltage probe (internal impedance: 500 MΩ) and a mixed domain oscilloscope (HVP, Tektronix MDO3000s).

Supporting Information

Supporting Information is available from the Wiley Online Library or from the author.

Acknowledgements

Conflict of Interest

The authors declare no conflict of interest.

Keywords

[1] M. B. Dastagiri, *Eur. Sci. J.* **2017**, *13*, 312.

[2] W. Li, B. Clark, J. A. Taylor, H. Kendall, G. Jones, Z. Li, S. Jin, C. Zhao, G. Yang, C. Shuai, X. Cheng, J. Chen, H. Yang, L. J. Frewer, *Comput. Electron. Agric.* **2020**, *172*, 105305.

[3] J. Ruan, H. Jiang, C. Zhu, X. Hu, Y. Shi, T. Liu, W. Rao, F. T. S. Chan, *IEEE. Wirel. Commun.* **2019**, *26*, 56.

[4] a) Z. L. Wang, *Nano Energy* **2019**, *58*, 669; b) W. Kim, D. Bhatia, S. Jeong, D. Choi, *Nano Energy* **2019**, *56*, 307.

[5] a) J. Nie, Z. Ren, L. Xu, S. Lin, F. Zhan, X. Chen, Z. L. Wang, *Adv. Mater.* **2020**, *32*, 1905696; b) S. Li, Y. Fan, H. Chen, J. Nie, Y. Liang, X. Tao, J. Zhang, X. Chen, E. Fu, Z. L. Wang, *Energy Environ. Sci.* **2020**, *13*, 896.

[6] F.-R. Fan, Z.-Q. Tian, Z. Lin Wang, *Nano Energy* **2012**, *1*, 328.

[7] C. Rodrigues, D. Nunes, D. Clemente, N. Mathias, J. M. Correia, P. Rosa-Santos, F. Taveira-Pinto, T. Morais, A. M. Pereira, J. Ventura, *Energy Environ. Sci.* **2020**, *13*, 2657.

[8] Z. L. Wang, *Mater. Today* **2017**, *20*, 74.

[9] a) W. Xu, H. Zheng, Y. Liu, X. Zhou, C. Zhang, Y. Song, X. Deng, M. Leung, Z. Yang, R. X. Xu, Z. L. Wang, X. C. Zeng, Z. Wang, *Nature* **2020**, *578*, 392; b) L. Xu, T. Jiang, P. Lin, J. J. Shao, C. He, W. Zhong, X. Y. Chen, Z. L. Wang, *ACS Nano* **2018**, *12*, 1849; c) I.-W. Tcho, S.-B. Jeon, S.-J. Park, W.-G. Kim, I. K. Jin, J.-K. Han, D. Kim, Y.-K. Choi, *Nano Energy* **2018**, *50*, 489; d) S. Adonijah Graham, B. Dudem, H. Patnam, A. R. Mule, J. S. Yu, *ACS Energy Lett.* **2020**, *5*, 2140.

[10] a) H. Ryu, J. H. Lee, U. Khan, S. S. Kwak, R. Hinchet, S.-W. Kim, *Energy Environ. Sci.* **2018**, *11*, 2057; b) Y. Wang, E. Yang, T. Chen, J. Wang, Z. Hu, J. Mi, X. Pan, M. Xu, *Nano Energy* **2020**, *78*, 105279; c) B. Dudem, N. D. Huynh, W. Kim, D. H. Kim, H. J. Hwang, D. Choi, J. S. Yu, *Nano Energy* **2017**, *42*, 269.

[11] a) R. Hinchet, H.-J. Yoon, H. Ryu, M.-K. Kim, E.-K. Choi, D.-S. Kim, S.-W. Kim, *Science* **2019**, *365*, 491; b) M. T. Rahman, S. M. S. Rana, M. Salauddin, P. Maharjan, T. Bhatta, J. Y. Park, *Adv. Energy Mater.* **2020**, *10*, 1903663; c) A. R. Mule, B. Dudem, S. A. Graham, J. S. Yu, *Adv. Funct. Mater.* **2019**, *29*, 1807779.

[12] a) Z. L. Wang, T. Jiang, L. Xu, *Nano Energy* **2017**, *39*, 9; b) J. An, Z. M. Wang, T. Jiang, X. Liang, Z. L. Wang, *Adv. Funct. Mater.* **2019**, *29*, 1904867; c) K. Xia, J. Fu, Z. Xu, *Adv. Energy Mater.* **2020**, *10*, 2000426.

[13] a) X. Xiao, X. Zhang, S. Wang, H. Ouyang, P. Chen, L. Song, H. Yuan, Y. Ji, P. Wang, Z. Li, M. Xu, Z. L. Wang, *Adv. Energy Mater.* **2019**, *9*, 1902460; b) Z. Ren, Z. Wang, Z. Liu, L. Wang, H. Guo, L. Li, S. Li, X. Chen, W. Tang, Z. L. Wang, *Adv. Energy Mater.* **2020**, *10*, 2001770.

[14] K. Saewon, C. Seungse, S. Ravi, L. Hochan, P. Jonghwa, U. Doo-Seung, L. Youngoh, K. Hyunhyub, *Sci. Adv.* **2018**, *4*, eaas8772.

[15] Z. Wang, J. An, J. Nie, J. Luo, J. Shao, T. Jiang, B. Chen, W. Tang, Z. L. Wang, *Adv. Mater.* **2020**, *32*, 2001466.

[16] a) J. Chen, Y. Huang, N. Zhang, H. Zou, R. Liu, C. Tao, X. Fan, Z. L. Wang, *Nat. Energy* **2016**, *1*, 16138; b) S. Dong, F. Xu, Y. Sheng, Z. Guo, X. Pu, Y. Liu, *Nano Energy* **2020**, *78*, 105327.

[17] Z. L. Wang, A. C. Wang, *Mater. Today* **2019**, *30*, 34.

[18] L. Lin, Y. Xie, S. Niu, S. Wang, P.-K. Yang, Z. L. Wang, *ACS Nano* **2015**, *9*, 922.

[19] T. Jiang, H. Pang, J. An, P. Lu, Y. Feng, X. Liang, W. Zhong, Z. L. Wang, *Adv. Energy Mater.* **2020**, *10*, 2000064.

[20] J. Chen, H. Guo, C. Hu, Z. L. Wang, *Adv. Energy Mater.* **2020**, *10*, 2000886.

[21] E. N. Jayaweera, K. R. Wijewardhana, T. K. Ekanayaka, A. Shahzad, J.-K. Song, *ACS Sustainable Chem. Eng.* **2018**, *6*, 6321.

[22] a) G. Haiqi, L. Bingjing, L. Han, Z. Zongcai, *Anim. Husb. Feed Sci.* **2018**, *10*, 81; b) X. L. Wang, L. S. Zhang, H. L. Liu, Z. Q. Du, W. D. Yu, *J. Donghua Univ.* **2016**, *33*, 66; c) K. E. Moore, D. Blache, S. K. Maloney, *Small Rumin. Res.* **2011**, *96*, 165.

[23] a) Y. Bai, L. Xu, C. He, L. Zhu, X. Yang, T. Jiang, J. Nie, W. Zhong, Z. L. Wang, *Nano Energy* **2019**, *66*, 104117; b) N. Zhai, Z. Wen, X. Chen, A. Wei, M. Sha, J. Fu, Y. Liu, J. Zhong, X. Sun, *Adv. Energy Mater.* **2020**, *10*, 2001041; c) Z. Liu, J. Nie, B. Miao, J. Li, Y. Cui, S. Wang, X. Zhang, G. Zhao, Y. Deng, Y. Wu, Z. Li, L. Li, Z. L. Wang, *Adv. Mater.* **2019**, *31*, 1807795.

[24] W. Liu, Z. Wang, G. Wang, G. Liu, J. Chen, X. Pu, Y. Xi, X. Wang, H. Guo, C. Hu, Z. L. Wang, *Nat. Commun.* **2019**, *10*, 1426.

[25] Q. T. Zheng, Y. Zhang, M. X. Yang, H. W. Liu, *Adv. Mater. Res.* **2011**, *332–334*, 1063.

[26] S. Lin, L. Xu, C. Xu, X. Chen, A. C. Wang, B. Zhang, P. Lin, Y. Yang, H. Zhao, Z. L. Wang, *Adv. Mater.* **2019**, *31*, 1808197.

[27] S. Niu, S. Wang, L. Lin, Y. Liu, Y. S. Zhou, Y. Hu, Z. L. Wang, *Energy Environ. Sci.* **2013**, *6*, 3576.